Apparent flow dimension approach to the study of heterogeneous fracture network systems

Kunwar Mrityunjai Sharma[1*], Benoit Dessirier[2], Chin-Fu Tsang[1,3], and Auli Niemi[1]
[1]Uppsala University, Department of Earth Sciences, Sweden
Email: mrityunjai.sharma@geo.uu.se
[2]Stockholm University, Stockholm, Sweden
[3]Lawrence Berkeley National Laboratory, Berkeley, CA, USA

Abstract

The generalized radial flow (GRF) model in well-test analysis employs non-integer flow dimensions to represent the variation in flow area with respect to radial distance from a borehole. However, the flow dimension is influenced not only by changes in flow area, but also by permeability variations in the flow medium. In this paper, the flow dimension from the combined effect of flow dimensionality and permeability/conductance variation is interpreted and referred to as apparent flow dimension (AFD). AFD is determined using the second derivative of the drawdown-time plot from pressure transient testing, which may have varied non-integer values with time. This paper presents a systematic set of investigations starting from idealized channel networks in one, two and three dimensions, and proceeding to a case study with a complex fracture network based on actual field data. Interestingly, a general relation between the AFD upsurge/dip and the conductance contrast between adjacent flow channels is established. The relation is derived from calculations for 1D networks but is shown to be useful even for data interpretation for more complex 2D and 3D cases. In an application to fracture network data at a real site, the presence of flow channel clusters is identified using the AFD plot. Overall, the AFD analysis is shown to be a useful tool in detecting the conductance/dimensionality changes in the flow system, and may serve as one of the different data types that can be jointly analysed for characterizing a heterogeneous flow system.

Keywords: Flow dimension, Channelling, Transient testing, Network systems, Site in Sweden

1. Introduction

Understanding the flow and transport in fractured rocks is critically important for a number of key geotechnical and hydrogeological applications. In fractured rocks the flow can vary from being relatively evenly distributed and space-filling to a system where most of the flow takes place in a few dominating channels. Various hydrological and rock mechanical processes act differently in these extremely different systems and therefore it is important to understand the prevailing flow system when doing any model predictions. Well testing is the technique for determining an aquifer's hydraulic properties. In well tests, a disturbance in pressure or flow is introduced in the test borehole and the propagation of this disturbance inside the formation is monitored in terms of head/pressure variation and the results interpreted using a suitable model representing the flow in the formation. The conventional well-test interpretation models assume an idealized flow geometry in a homogeneous and infinite domain, such as the radial/cylindrical flow model by Theis (1935), the linear flow model by Miller (1962), and the radial-to-spherical flow model by Moye (1967). Diagnostic plots in log-log scale showing the drawdown and its logarithmic derivative as a function of time are often used in well-test analysis (Bourdet et al., 1983). The concept of the use of logarithmic derivatives in the interpretation of well test results was introduced by Chow (1952), who presented a graphical method to determine the formation constants of an artesian aquifer from pumping test data. The logarithmic derivative is highly sensitive to minor changes in the variations of hydraulic head and therefore enables the detection of behaviours that would be difficult to notice using the drawdown curve only. To account for more complex hydrogeologic systems, especially encountered in fractured rocks, Barker (1988) proposed a so-called generalised radial flow (GRF) model. In this method, an additional parameter named flow dimension was included, which is the second derivative of the drawdown-time plot. Unlike the earlier models, this model accounts even for non-integer flow dimensions. Flow dimension reflects the network's flow geometry by indicating how the cross-sectional area to the flow varies in relation to the distance from the testing well and can have non-integer values different from one, two or three. The flow-dimension diagnostic plots inspired some simple approaches as a replacement of specialized models, for example Delay et al. (2004) presented a new analytical method using Gauss-Newton algorithm to study the interference pumping tests in Poitiers, France.

Doe and Geier (1990) were among the first ones to apply the GRF model for the analysis of field data to identify the flow geometry of the fracture system and at the Stripa mine, Sweden, at about 360 m depth. The impact of boundary effects was observed to be negligible indicating a well-connected fracture system. The spatial dimension interpreted from the tests varied from sub-linear (conductivity decreasing with distance from the hole) to spherical for a three-dimensional dense fracture system. During certain pressure tests, the flow dimension also varied over time. Doe (1991) further discusses the use of the GRF method in terms of the interpretation of constant-pressure well tests and points out that flow dimension also reflects aquifer conductivity heterogeneity and that flow geometry and conductivity heterogeneity are actually interchangeable in the interpretation of flow dimension. This was identified as a shortcoming of the GRF technique, but can also been seen as an opportunity, as the method nevertheless allows to investigate different underlying conceptual models for flow, as pointed out e.g. by Walker and Roberts (2003). Kuusela-Lahtinen et al. (2003) analysed a large data set from a low-conductivity crystalline rocks down to 450 m depth from the Finnish nuclear waste investigation programme. The results showed that the lower dimensions corresponding to linear and sub-linear flow were easy to distinguish from dimensions over 2, while the dimensions 2 to 3 were more difficult to distinguish from each other. The latter was usually because of practical difficulties in creating accurate early-time data, as required by the theory. The results nevertheless gave good indications as of how flow dimension varied both with the scale of the measurement (2m or 10m), the depth of the investigation and the character of the rock (fracture zone or average rock). Renard et al. (2009) discussed the merits and demerits of using flow dimension diagnostic plots with the help of three field examples and advised for caution due to their high sensitivity to small variations in drawdown which can lead to misinterpretations. They emphasized that due to the certain degree of non-uniqueness in the interpretation, the information on flow dimension must be combined with other information obtained from geological, geophysical, and hydrological data, in order to build a valid fracture network model.

Gringarten (2008) and Ferroud et al. (2018) evaluated the historical development of flow dimension study in aquifer characterization. Cello et al. (2009) examined the relationship between DFN parameters and flow dimension by applying Monte Carlo analysis. Verbovšek (2009) performed the flow dimensional analysis to correlate the flow dimension with hydraulic conductivities in the case of dolomites. The correlation was found to be poor. They also compared the flow dimension with fractal (Euclidian) dimension in 3D, and found flow dimension to be always less than its fractal dimension. Odling et al. (2013) investigated the effect of flow dimensionality on flow and transport properties in the non-radial flow domain. They highlighted the significance of recognizing non-radial flow regime when estimating aquifer parameters and interpreting tracer breakthrough curves. Additionally, they noted that disregarding the existence of non-radial flow in the case of partly penetrating boreholes might result in an overestimation of aquifer parameters. Ferroud et al. (2019) performed a thorough investigation of well test data from different geologic settings and observed that in addition to the prevalence of cylindrical-radial flow, non-cylindrical-radial flows are also common and may change in the course of a well test. According to them the non-cylindrical-radial flow dimensions ($n < 2$, or $n > 2$) can be easily recognised. This is also reported by other investigators (Cinco et al. 1978; Kuusela-Lahtinen et al., 2003, Kuusela-Lahtinen and Poteri 2010; Rafini et al. 2017).

In spite of the extensive work since the first development of the GRF model, a systematic study combining the effects of flow dimensionality and permeability heterogeneity is presently lacking. With this in mind, this study presents a set of model analyses, starting from one dimensional channel models and proceeding to two- and three-dimensional systems, and investigates what an analysis of the flow dimension, or the apparent flow dimension AFD, from a flow test can tell about the characteristics of the system. We investigate the effect of conductance contrast between the connected flow channels in a constant flow transient well test with the objective of formulating a relationship between conductance contrast and the AFD. The term AFD is used in the following text to indicate the fact that we are analysing it from the observed well test, which combines not only the effect of variable flow dimension but also the effect of permeability/conductance contrast.

2. Methods

A channel network model, CHAN3D, was developed by Gylling et al. (1999), which uses a lattice channel network to represent a system of fractures where each node is connected to six adjacent nodes and the channel conductance follows log normal distribution (Gylling et al., 1999; Moreno & Neretnieks, 1993). This model was later enhanced to include more complex parameters such as stagnant water zones and rock matrix layer properties in tracer transport (Mahmoudzadeh et al., 2013; Moreno et al., 2006; Neretnieks, 2006; Shahkarami et al., 2016).

Our study uses a further development of the code by Dessirier et al. (2018), who modified the model to automatically generate lattice networks as described by Gylling et al., (1999) and sparse lattice networks as defined by Black et al. (2017). The resulting script, *pychan3D* code, also includes a customizable method to build unstructured networks from scratch, amend existing networks, and apply boundary conditions as well as to select different numerical solvers and to export the results for 3D visualization. For the present work this code was further developed to include the transient test in the fracture network. It should be pointed out that even though the structure of the code is that of channel network, it can be used to model uneven flow in fracture planes and three-dimensional fracture networks, where small channel sections with different properties can be used to represent local flow heterogeneities in fracture planes.

In the following text we will describe shortly the essential features of the model, for both steady state and transient simulation, followed by how the actual apparent flow dimension is determined from the results of the transient pressure-flow simulations.

2.1 Model for steady state groundwater flow

In *pychan3D* model (Dessirier et al., 2018), the steady state flow rate (Q) along a channel with conductance C and head difference (Δh) at the two ends is formulated as:

$$Q = C \cdot \Delta h \tag{1}$$

The conductance of a channel with average transmissivity (T), width (w) and length (L) in simple rectangular cross section can be defined as:

$$C = \frac{T \cdot w}{L} \tag{2}$$

The head h at every point in the network can then be solved form a linear system of equations by introducing a Laplacian matrix in mass balance equation at each node (Li et al., 2014).

$$M_c \cdot h = B_c \tag{3}$$

Where, Mc = Laplacian matrix of the network of conductances;

B_c = vector of boundary conditions

2.2 Transient flow formulation

Analysis of flow dimension requires transient flow simulations, for which the model by Dessirier et al. (2018) was further developed. For this we assume, as before, one-dimensional channel length extending from x=0 to x= L, of width w, conductance C, and now also with constant storativity S. Taking note of the Laplace variable p, the channel's ability to adjust to changes in conditions at its two ends can be represented by an effective distance (x_p).

$$x_p = \sqrt{\frac{C \cdot L}{p \cdot S \cdot w}} \tag{4}$$

where the subscript shows the Laplace variable dependency. Then, the pressure head can be shown in the Laplace domain as a function of the initial head $h_i(x)$ and the pressures at the ends of the channel $H_0(p)$ and $H_L(p)$.

$$H(x,p) = \frac{h_i(x)}{p} + \frac{\left[H_L(p) - \frac{h_i(L)}{p}\right] \cdot sin\,h\frac{x}{x_p} + \left[H_0(p) - \frac{h_i(0)}{p}\right] \cdot sin\,h\frac{L-x}{x_p}}{sin\,h\frac{L}{x_p}} \quad (5)$$

This analytical solution enables the calculation of transient flow variables at the channel ends:

$$Q_0(p) = -C \cdot L \cdot \frac{\partial H(x,p)}{\partial x}\Big)_{x=0} \; and \; Q_L(p) = -C \cdot L \cdot \frac{\partial H(x,p)}{\partial x}\Big)_{x=L} \quad (6)$$

Considering the vector of the transient pressure values being unknown at the network nodes, the matrix formulation of the steady state problem can be extended to the transient problem in the form of Laplace space.

2.3 Determining the flow dimension

After obtaining the flow solution in time domain for a pumping test, the pressure drawdown/ build up curve can be used to determine the apparent flow dimension near the pump. With the help of pressure drawdown/build-up (h) at the well, the pressure derivative (h') and slope of pressure derivative are expressed as shown in equations 7 and 8 as follows. Also notice that the unit of the pressure derivative will be the same as the pressure itself since it is a log derivative.

$$h' = log\frac{dh}{dlnt} \quad (7)$$

$$v *= \frac{dh'}{dlogt} \quad (8)$$

The flow dimension n of the system can then be formulated as (Barker, 1988):

$$n = 2(1 - v*) \quad (9)$$

In other words, the slope (v*) between h' and log t is used to determine the flow dimension. For linear flow the integer flow dimension becomes n=1 (v*=0.5), for radial flow n=2 (v*=0) and for spherical flow n=3 (v*= -0.5) The fractional flow dimension values other than these three values are also possible and can represent realistic flow systems (Walker et al., 2006).

To exemplify how flow dimension appears in a log-log plot between pressure derivative (h') and time, Fig. 1 gives some examples of published flow dimension values (Cinco et al., 1978; Gringarten et al., 1974; National Research Council, 1996; Rafini & Larocque, 2009). Additionally, the flow dimensions at different boundaries are also shown, with n=4 representing a constant head boundary and n=0 a no-flow boundary (Fig. 1).

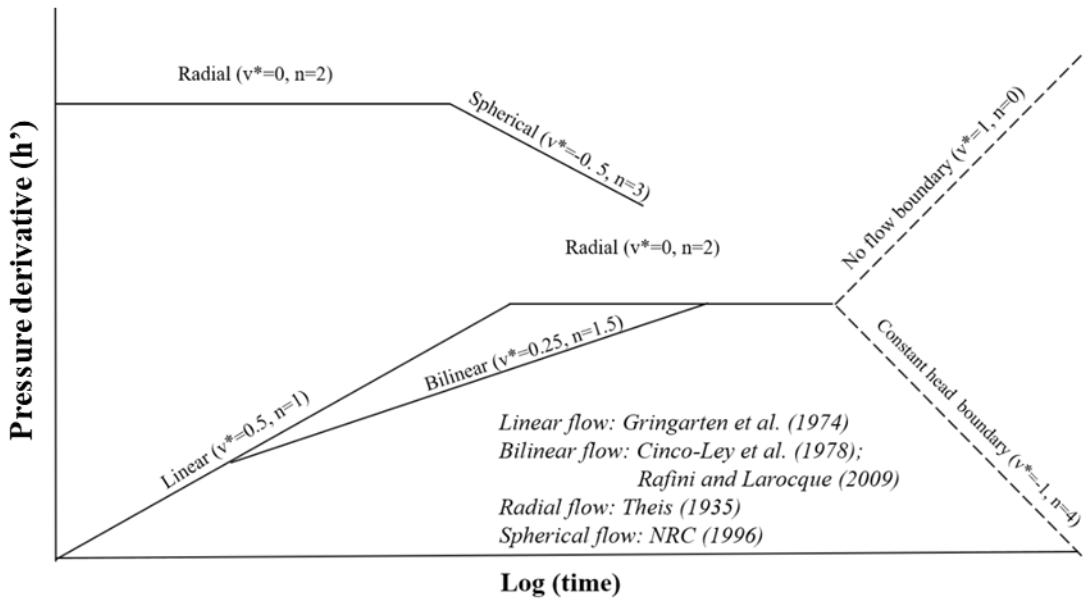

Fig. 1 Examples of flow regimes and flow dimension presented in the literature

3. Results

3.1 One Dimensional Channel and Effect of Conductivity Contrast on Apparent Flow Dimension

As a first case, the simplest possible model consisting of one-dimensional channels was considered. A systematic analysis of flow in 1D channels can provide useful insight assisting the analysis of later more complex two- and three-dimensional channel networks.

3.1.1 Effect of conductance contrast on flow dimension

The simplest model (Fig. 2) consists of two sections having conductances C1 and C2 respectively. In the Figure, N0 is the injection node, N1 is a junction between sections of two conductances and N2 is a closed boundary node. Steady state solution is first acquired by applying constant pressure at the boundary of the network and then the system is used to test the transient response by imposing a constant flow injection at the injection node with a closed outer boundary.

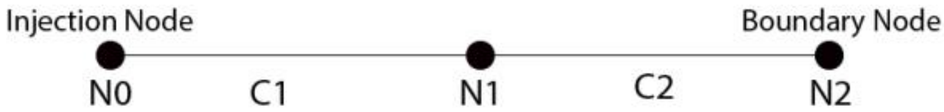

Fig. 2 Simple 1D channel network with three nodes and two channels

Fig. 3 shows the pressure, its derivative and the apparent flow dimension (n) for different conductance contrast. When C1/C2 =1, we have two channels with same conductance and the AFD plot is presented in Fig. 3(d), showing a constant flow dimension of n=1 which drops to n=0, indicating the effect of the closed boundary node. Fig. 3(a) demonstrates the case with C1/C2=1000 (highest drop in conductance). Here AFD initially starts with value n=1 (indicating linear flow), then dips suddenly indicating the presence of the conductance contrast at C1-C2 junction but then reverts again to its initial value n=1. Then at a much later time, as before, it drops again to zero due to the effect of the closed boundary. In the rest of the sub-figures under Fig.3 we can see that AFD changes abruptly at the conductance contrast in each case. Depending on whether a higher or lower conductance is encountered, there is an abrupt peak or dip of the apparent flow dimension at the conductance contrast, with AFD increasing above n=1 when C1< C2, and falling below n=1 when C1>C2. Furthermore, it can be seen that the magnitude of the peaking and dipping in ADF correlates well with the magnitude of the conductance difference (Fig. 4).

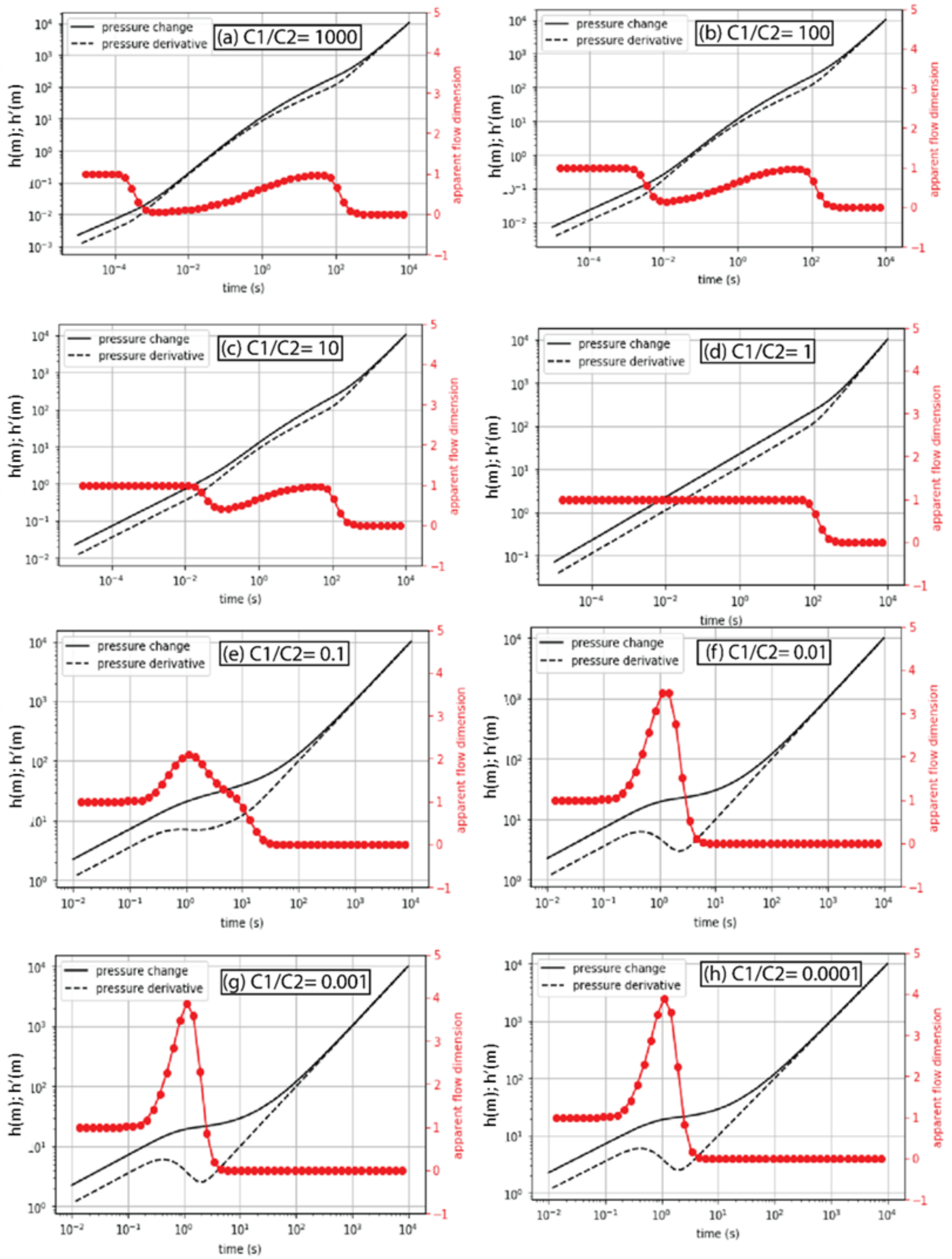

Fig. 3 Pressure (h), its derivative (h') and Apparent flow dimension (n) during a constant rate injection test along the two-conductance network with a no-flow far boundary

Fig. 4 shows the peak/dip of AFD value as a function of the conductance contrast C1/C2 and we can see a clear correlation. This kind of a general relationship between the AFD peak or dip and the conductance contrast is found to be useful (see below) even when analysing the behaviour of more complex multidimensional channel networks.

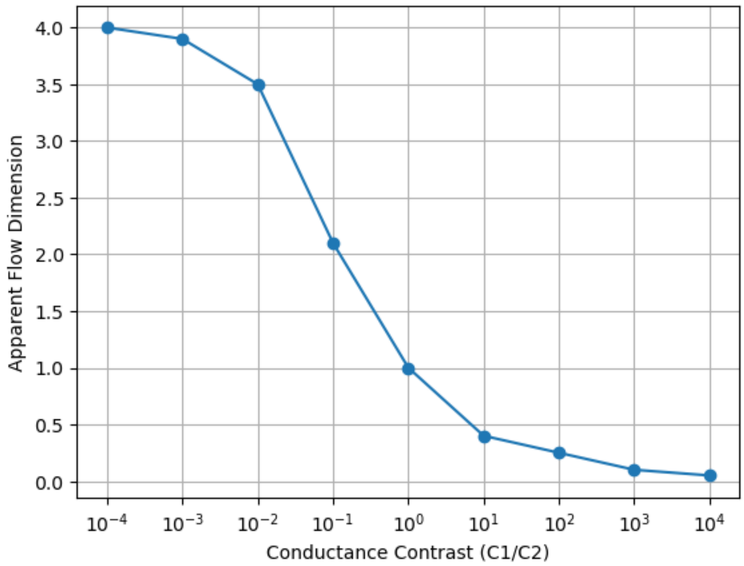

Fig. 4 Relationship between the peak/drop in AFD and the conductance contrast (C1/C2)

Next, a three-section channel network is built (Fig. 5a) to examine the simultaneous effect of conductance increase and decrease within the same channel and also to verify the relationship established earlier in Fig. 4. The conductance of first and third sections, C1 and C3 are the same and the conductance of the middle section is varied. For the first case, the conductance of the middle section is *decreased* by two orders of magnitude, and the transient response of the network is then observed. In this case (Fig. 5b) we can observe that the AFD starts with value n=1 as expected and then drops to n=0.2 at the junction between C1 and C2, then attempts to recover its value of 1 again. At the C2-C3 junction with two orders of magnitude increase in conductance, AFD rises to value n=3.1 and then drops to zero at the boundary. These value pairs are in good agreement with the trend in Fig. 4. In the second case, conductance of the middle section of the network is instead *increased* by a hundred times and transient response is again observed (Fig. 5c) Similarly, at C1-C2 junction with two order of magnitude increase in conductance, AFD rises to n=3.5, and again drops to 0.2 at similar decrease in conductance. In other words, when the conductance contrast (C1/C2) is compared to the AFD upsurge (n=3.1 and 3.5) or dip (n=0.1 and 0.2), the result is in a good agreement with the generalized relationship depicted in Fig. 4. It also confirms that the AFD behaviour in the three-section example is consistent with the earlier two-section case.

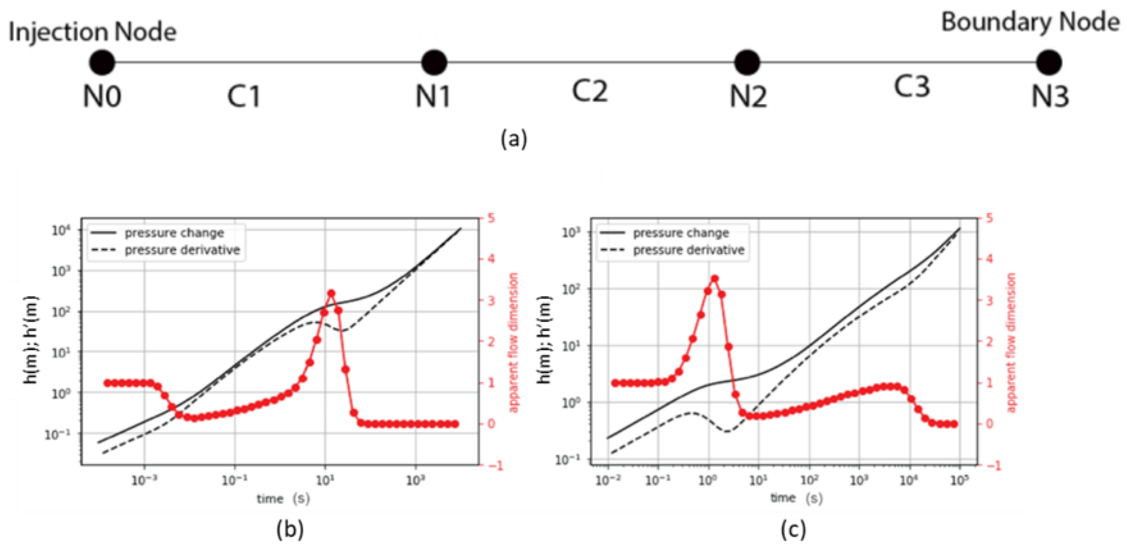

Fig. 5 (a) 1D network with three sections. Pressure (h), its derivative (h') and Apparent flow dimension (n) during a constant rate injection test along the network with conductance contrast (b) C1/C2=100, and (c) C1/C2=0.01, with a no-flow far boundary

3.2 Two-Dimensional Channel Network with statistical heterogeneity (σ = 1, 2, and 3)

As the next step, 2D channel networks were studied. For this, a 60x60 lattice of channels with conductance following an uncorrelated lognormal distribution were created with mean conductance of 10^{-10} m^2/s and four different standard deviation values: $\sigma = 0$ (homogeneous case), 1, 2 and 3. A standard deviation in log conductance of 3 in this case means a variance of conductance value of 3 (where the variance is the ratio of standard deviation in conductance to the mean conductance value). A larger standard deviation corresponds to a greater variation in conductances within the channel network and thereby a higher degree of heterogeneity. Fifty realizations were generated for each sigma value by means of random value generator built-in numpy, python library. A constant flow injection test was then simulated in these cases, with the injection well located at the centre of flow domain and a constant head boundary condition assigned to the outer circular boundary as shown in Fig. 6. Constant injection with injection rate of 7.2 m^3/hour for a duration of 3 hours, is simulated for the 50 realizations for each σ value.

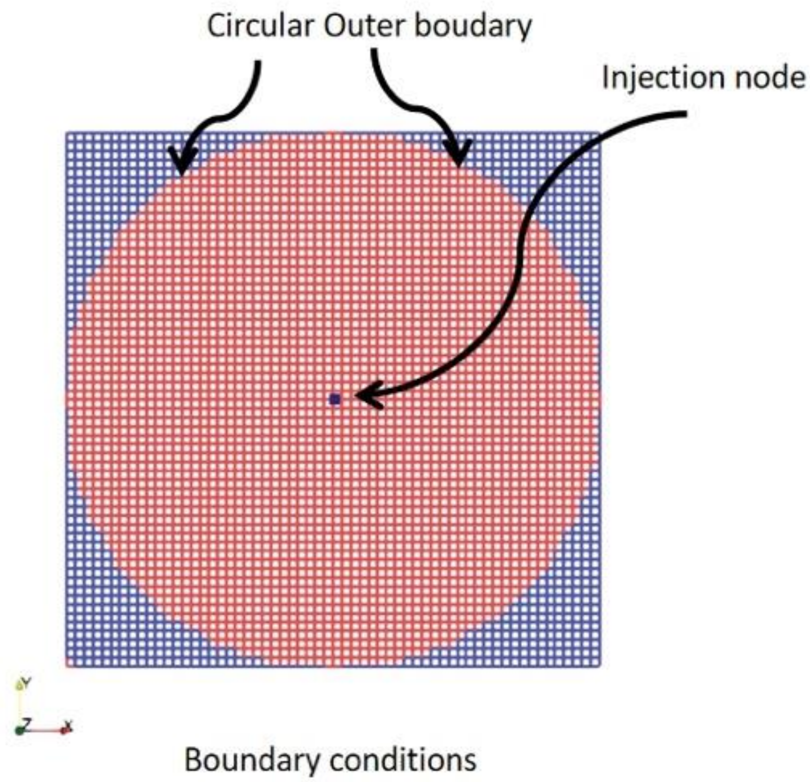

Fig. 6 Two-Dimensional channel network with boundary condition

Fig. 7 illustrates the obtained apparent flow dimension for all 50 realizations as a function of time for each of the σ = 1, 2, and 3 cases. For comparison the homogeneous case (σ=0) is also shown in all figs. It can be seen that for the homogeneous case the flow dimension always starts from a value of 1, indicating an early-time channelized flow when the flow is taking place in individual channels. After that there is a transition period followed by a long stable stage of 2-dimensional (cylindrical) flow, indicating that the flow is taking place radially throughout the system. Finally, a sharp increase to a high flow dimension is encountered when the flow encounters the constant pressure boundary. In contrast, results for σ = 1, 2, and 3 cases display a strong oscillatory behaviour in AFD, indicating the pressure front encountering steps of conductivity contrasts.

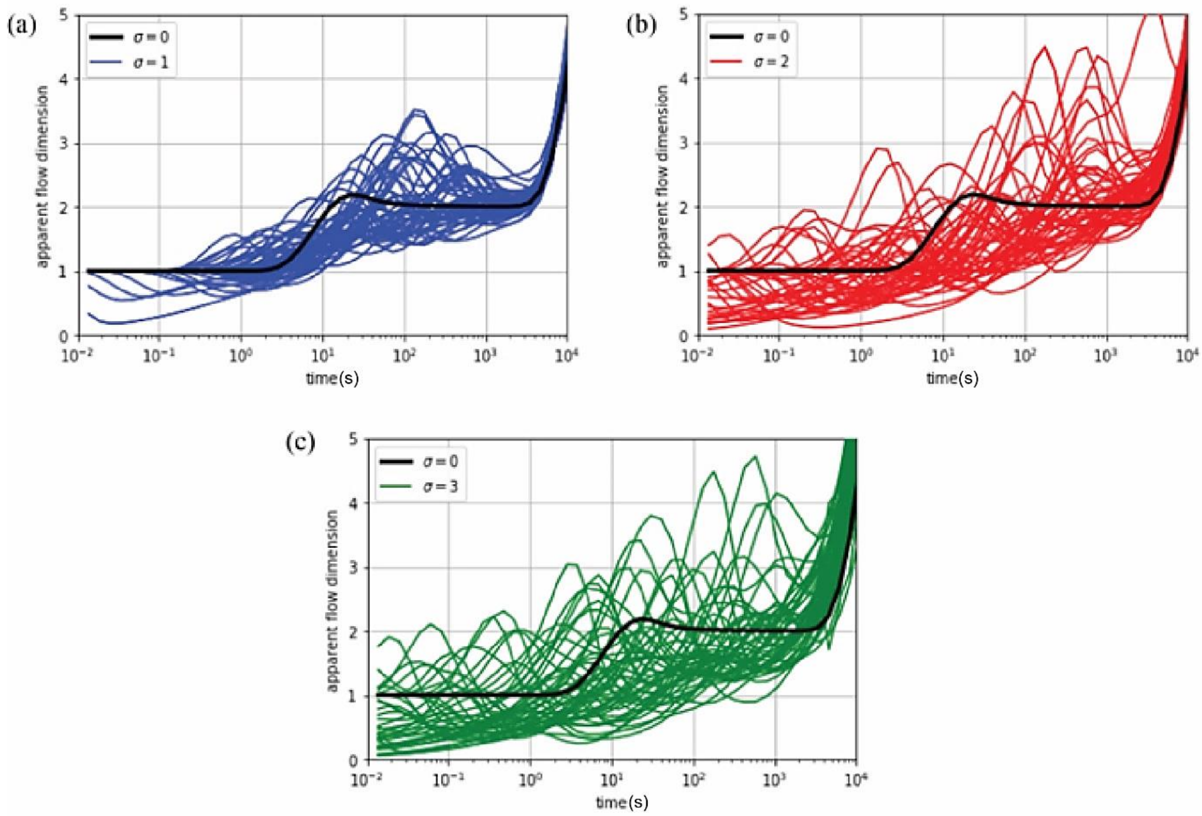

Fig. 7 AFD variation over time for three realisations having (a) σ=1, (b) σ=2, and σ =3

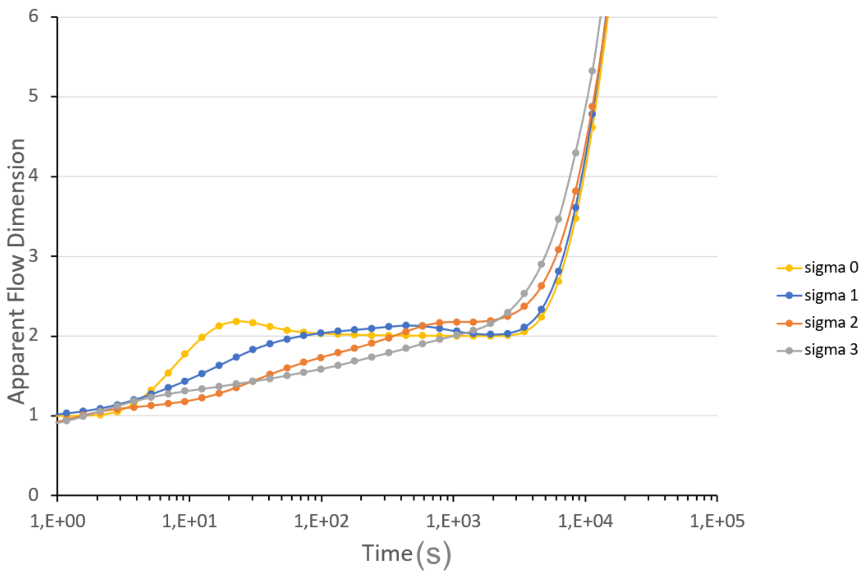

Fig. 8 Mean Apparent flow dimension for 50 realisations as a function of time

In Fig. 8 the arithmetic mean of AFD from all 50 realizations is shown for each σ. The figure implies that with an increase in σ, flow is taking more time to stabilize to the value of AFD=2 that indicates cylindrical flow. The flow dimension for higher σ values does not stabilize properly at value AFD=2 and ranges between 1 and 2 indicating a persistent bilinear flow behaviour. This points to the dominance of flow in sparse channels. Heterogeneity of the conductance field tends to reduce the expected apparent flow dimension and speed up the propagation of the pressure signal to the boundaries of the model, which are two of the characteristics of the channelling effect. For the individual realizations with $\sigma>0$ the behaviour is much more heterogeneous and characterized by a number of sharp fluctuations. The number of the fluctuations in the flow dimension as well as their magnitude increases when σ increases. The number of distinct AFD fluctuations around the mean for each σ and the root mean square (RMS) of AFD deviations from the mean is presented in Fig. 9 as a measure of the amplitude of AFD fluctuations. The increase of the amplitude of AFD fluctuation with an increase in the σ value is clearly seen in this figure, and further study will be made to explore its possible use in the estimation of the σ value of the underlying heterogeneity of the flow domain.

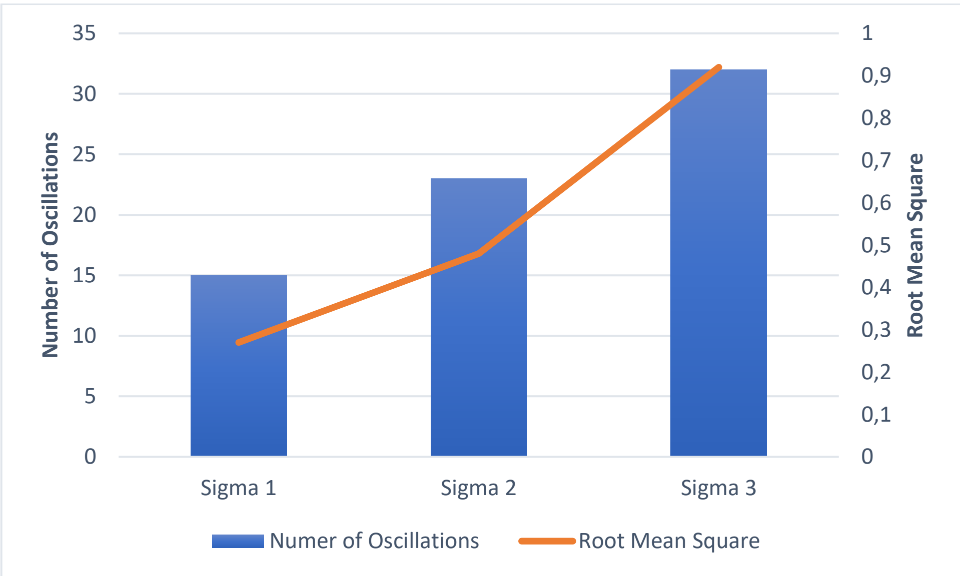

Fig. 9 Number of Oscillations and Root Mean Square of AFD deviation for each σ case

In Fig. 10, the steady state flow for one example realization is shown for the two standard deviations σ=1 and σ=2, to visually examine the appearance of channelization in them. It can be seen that the flow is more evenly distributed in the σ=1 case whereas in the σ=2 case it is concentrated into a smaller number of channels.

Flow rates for both sigma values and three example realisations from transient simulations at the time when the flow dimension becomes stable (at $t=10^3$ seconds) is shown in Fig. 11. From the flow rate distribution, it is visually evident that the flow gets more channelized with an increase in σ in all three realizations. In all the statistically heterogeneous cases, the flow dimension gets stable at the value lower than the corresponding Euclidian dimension, which also indicates the channelling phenomenon in the system.

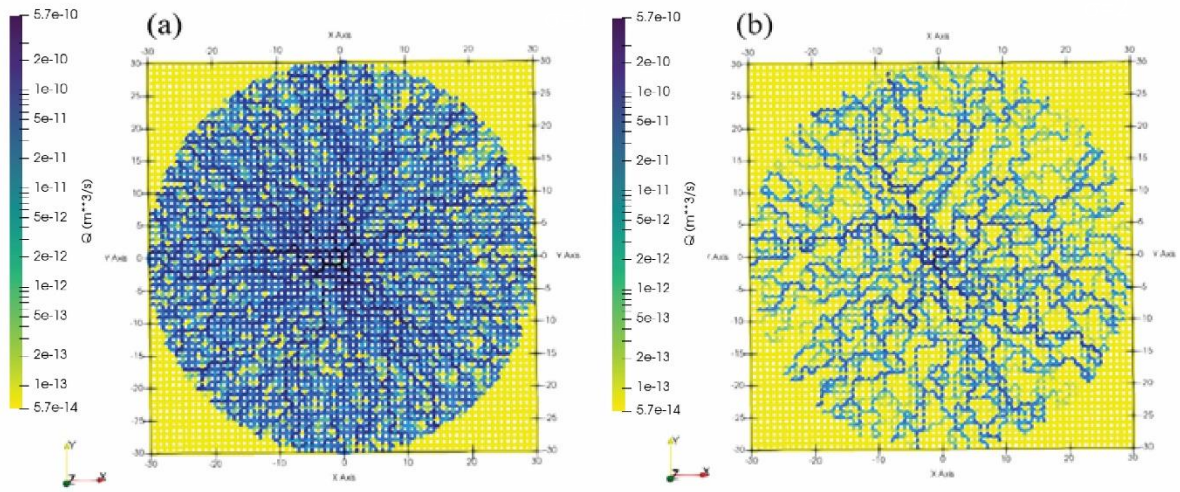

Fig. 10 Steady state flow rate for the 2-dimensional networks with conductance distribution a) σ=1 and b) σ=2

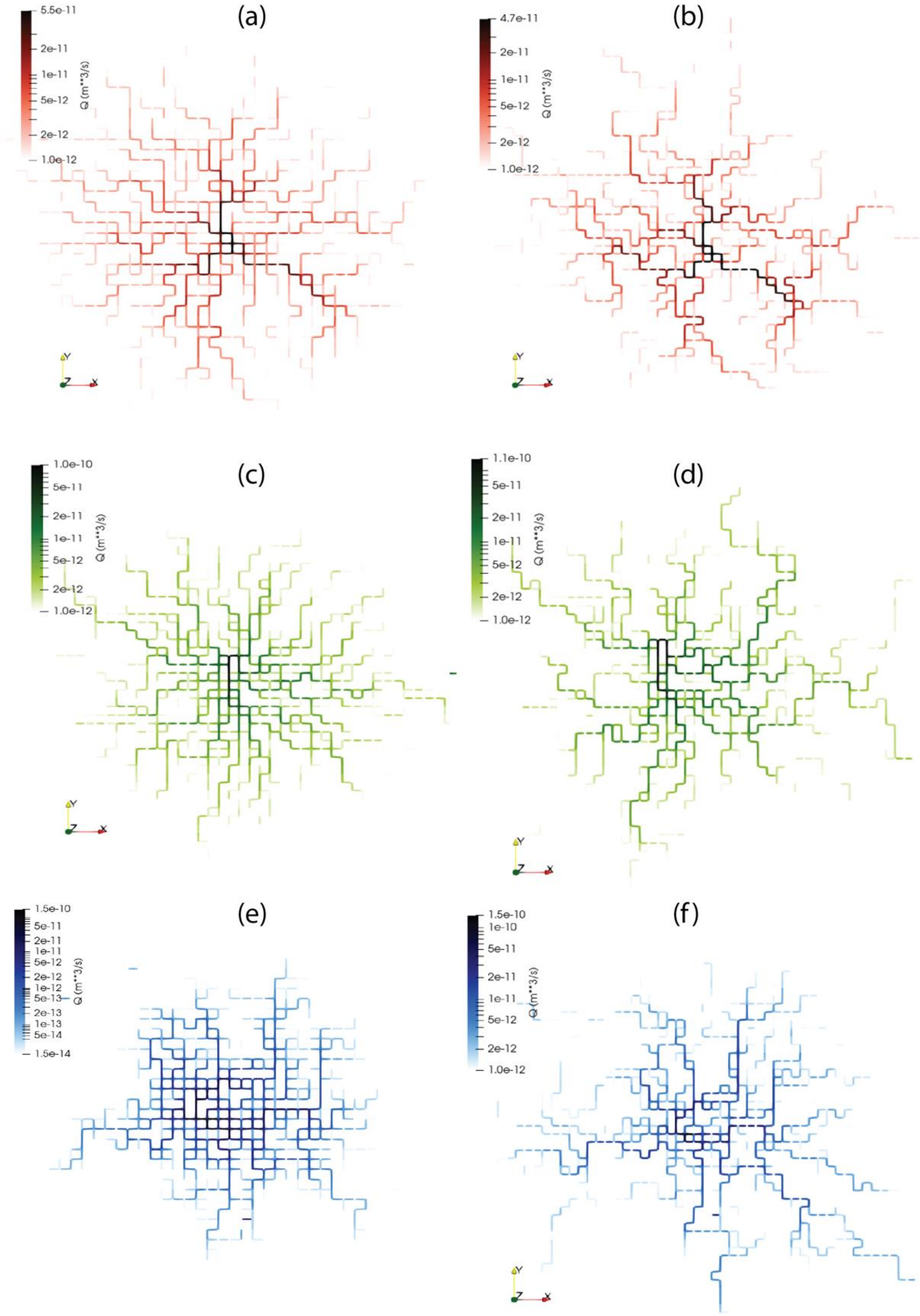

Fig. 11 Flow rate distribution at t=1000 seconds (a) σ=1, first realization, (b) σ=2, first realization, (c) σ=1, second realization (d) σ=2, second realization(e) σ=1, third realization (f) σ=2, third realization

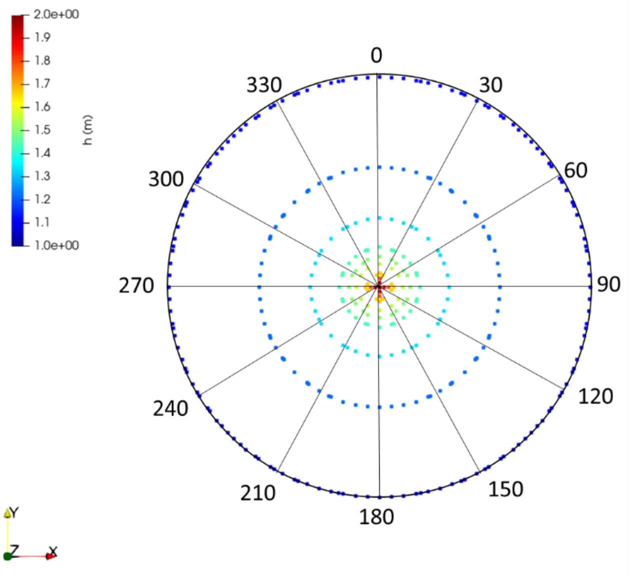

Fig. 12 Circle overlapping the pressure contour for an example realization of homogeneous conductance at t=1000 seconds

To determine the degree of channelization in a more quantitative way the flow domain was divided into sections of 30 degrees as shown in Fig. 12 and the number of channels intersecting an imaginary circle in each section was calculated. The radius of the imaginary circle was chosen by looking the pressure contour at the time t=1000 seconds from the homogeneous conductance case (the time when the flow dimension in the homogeneous case stabilizes). The number of channels intersecting the circumferential divisions are shown in Fig. 13. In all three realisations, the number of active channels intersecting the outer circumferential boundary is significantly reduced in case with σ=2 as compared to case with σ=1. The difference is especially pronounced in the case of the second realization (Fig. 13b), where most of the flow channels disappear and the most dominant flow channels are found in the direction between 270^{o} to 360^{o}.

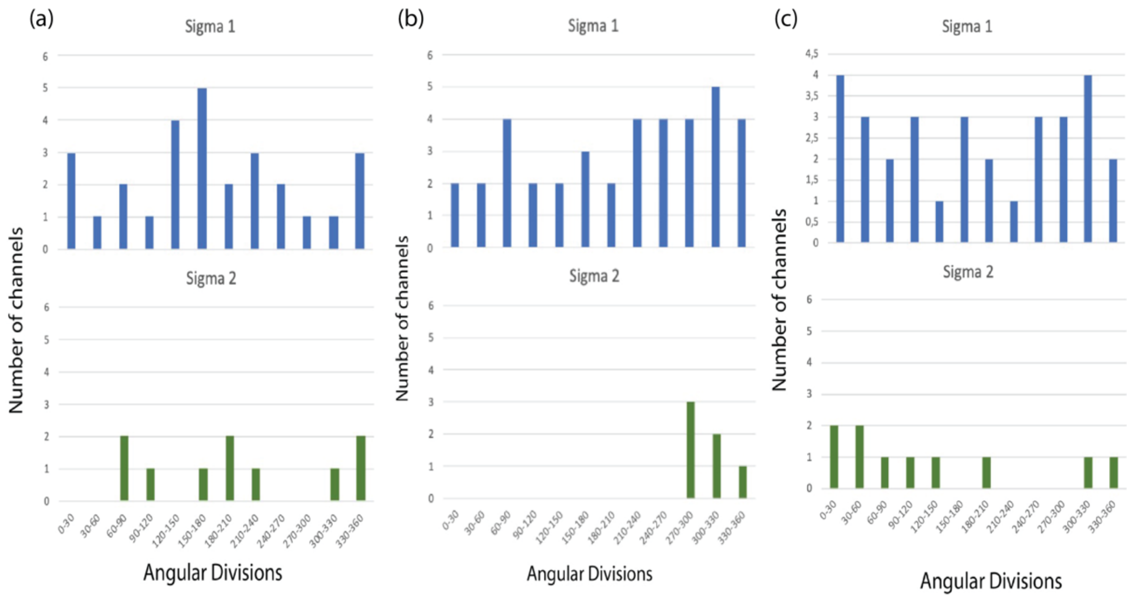

Fig. 13 The number of channels intersecting the circumferential boundary divisions for three realizations (a), (b) and (c) for σ1 and σ2

3.3 Two-Dimensional channel network with a linear high-conductance zone

In this subsection, the effect of a geometrically-defined, deterministic heterogeneity in the previous 2D stochastically heterogeneous flow domain is investigated. A linear zone where the channel conductances are increased 1000 times is introduced into a rectangular lattice (Fig. 14a and b). The linear high conductive zone may represent a deterministic feature such as a large fracture or fault zone. The conductance of the rest of the network is distributed log-normally as before, with standard deviation of either $\sigma=0$ (homogeneous case) or $\sigma=1$. The effect of the outer boundary on the transient test was also investigated by applying two different boundary conditions at the outer boundary; a constant pressure boundary representing an open outer boundary as well as a closed outer boundary. For the constant-pressure boundary case the simulated steady state pressure distributions for a sample realization for both conductance distributions ($\sigma=0$ and $\sigma=1$) shown in Fig.14c and d. A uniform circular pressure distribution around the injection point is observed for the homogeneous conductance case ($\sigma=0$), skewing away from the linear zone of higher conductance where pressure drop is instantaneous. In the heterogeneous case ($\sigma=1$) similar behaviour can be seen at the high permeability zone but now the hydraulic head distribution is not circular but shows local heterogeneity effects.

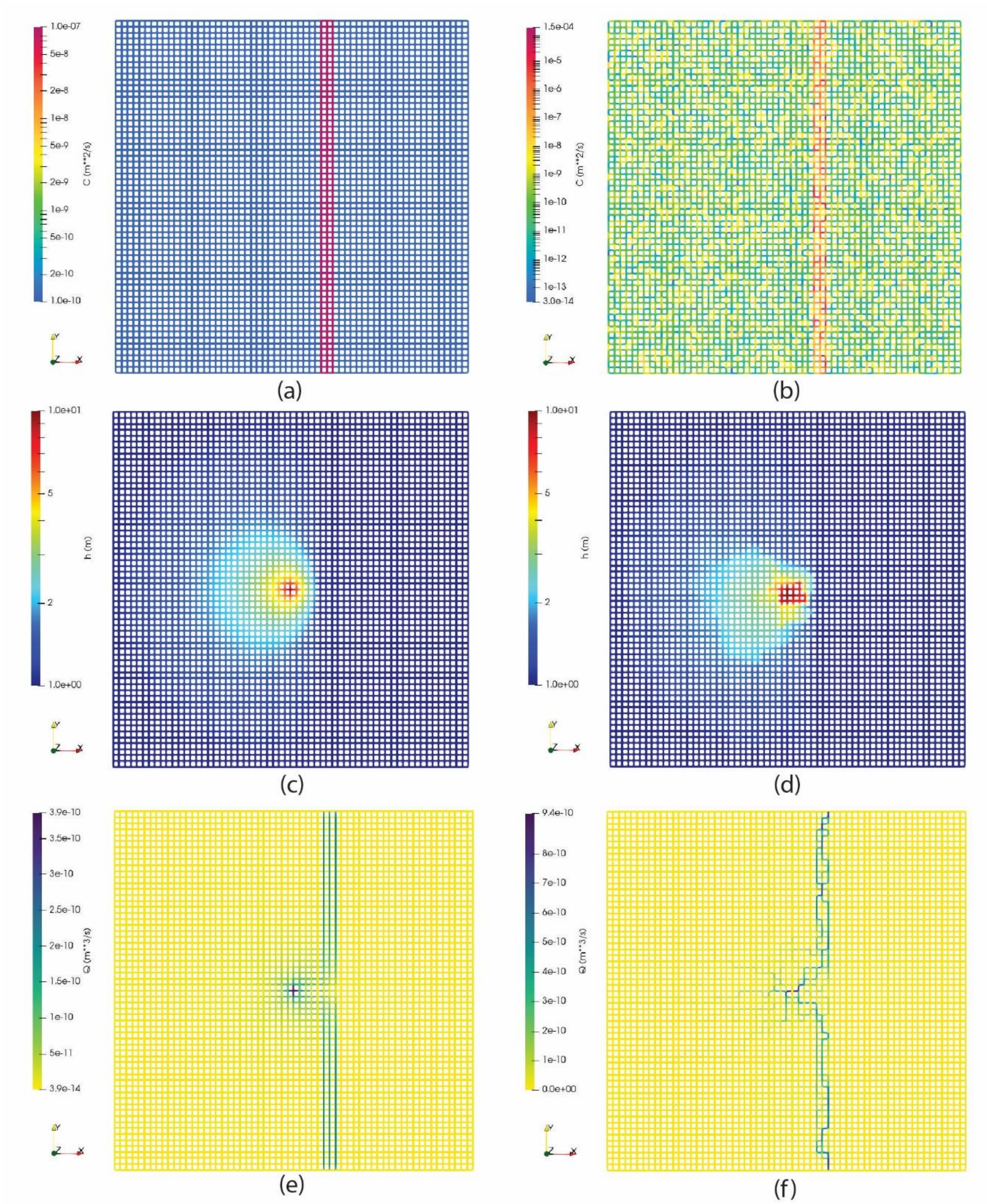

Fig. 14 (a) Rectangular lattice network with log normally distributed conductance, σ=0, and (b) σ=1 with a linear zone of higher conductance. (c) Simulated hydraulic head distribution, σ=0, and (d) σ=1. (e) Flow rate distribution, σ=0, and (f) σ=1.

Fig. 14 (e and f) demonstrates the steady state flow rate distribution in the two cases. The effect of the deterministic high-conductivity zone dominates the flow pattern in both cases. The flow initiates from the centre injection node and follows an outward trajectory towards the outer boundaries, until reaching the deterministic fault zone after which most of the flow preferentially follows the high-conductive channels towards the outer boundary. This is evident in both cases. In the heterogeneous case (Fig. 14 f), flow is even channelized within the deterministic high-conductance zone. Two degrees of channelization can be observed in this case; the primary channel of high flow occurs along the high conductance linear zone and the secondary channelization appears within the linear zone, due to the local conductance distribution with σ=1.

The effects of these geometrically defined heterogeneous systems during a transient well-test is examined next, in order to study how the various heterogeneity effects can be observed. A constant flow injection test using both open and closed outer boundary conditions is simulated in both geometries. Fig. 15 shows the AFD evolution with time for the two geometries (with conductance distributions of σ=0 and σ=1), for both open and closed outer boundary conditions. Fig. 15 (a) and (c) show the results for the uniform conductance σ=0, for open and closed boundary, respectively. At the open boundary, the AFD goes to a very large value when the pressure front reaches the boundary whereas at the closed boundary AFD drops to zero. We can see that AFD in both cases starts with n= 1, corresponding to the flow in channels in the immediate vicinity of the injection point. It then stabilizes at n=2, as expected in a 2-dimensional, radial domain. Next, when the flow encounters the high-conductivity zone Fig. 15(c), the AFD increases to 3.8, as a result of the three orders of magnitude increase in the overall conductivity. This observation is consistent with the observed correlation between conductance contrast and AFD found earlier in the case of the one-dimensional channels (Fig. 4). Similarly, for the case with non-uniform conductance distribution σ=1 (Fig. 15b and d), AFD starts with n=1, but varies with time depending on what channel conductivity is encountered and no stable 2D flow is reached (Fig. 15b and d). For this σ value, the presence of the high-conductivity zone is also seen in Fig. 15d as the AFD=3.8 peak.

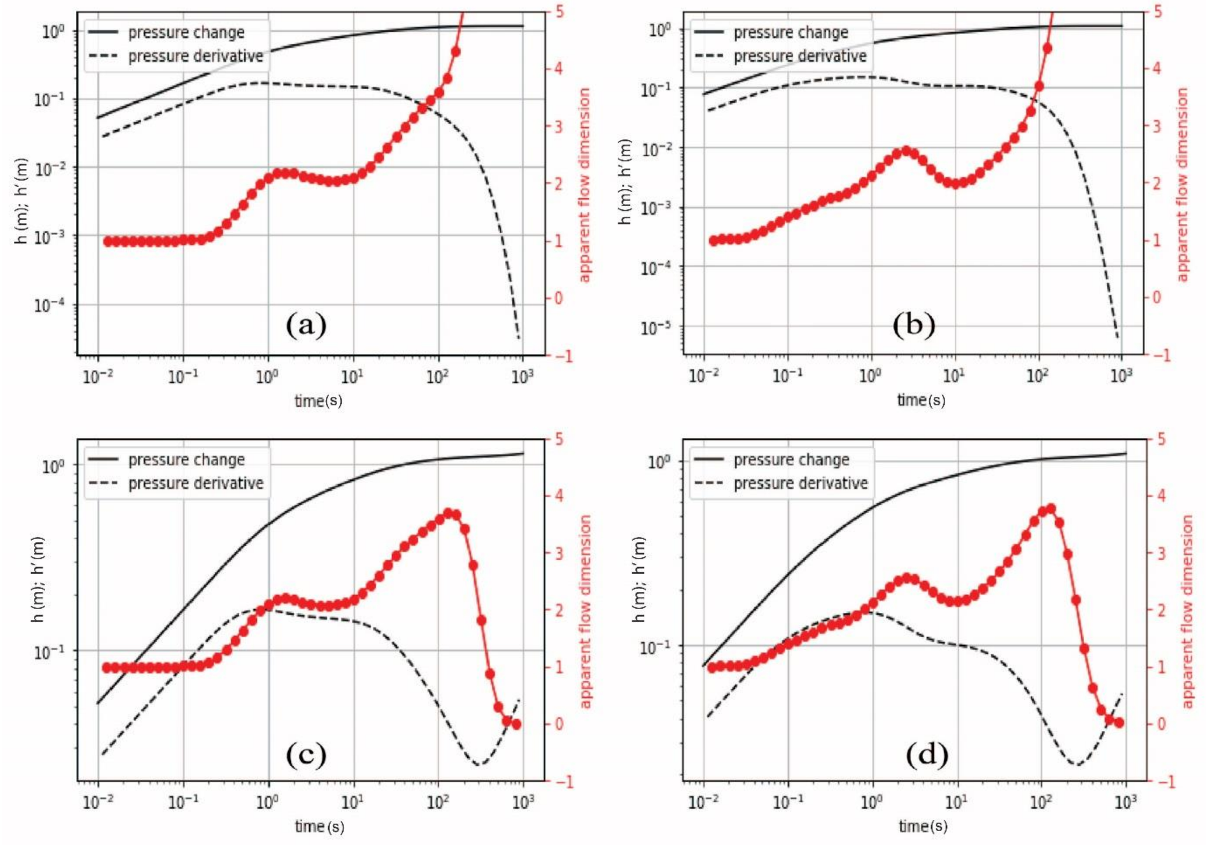

Fig. 15 AFD plot from transient test in (a) uniform conductance case (σ=0), (b) non-uniform conductance case with constant head boundary (σ=1), (c) uniform conductance case with closed boundary (σ=0), and (d) non-uniform conductance with closed boundary (σ=1)

3.4 Three-Dimensional Channel Network

After studying the 1D and 2D networks, similar concepts are extended to the 3D channel networks to check the validity in 3D domain. A channel network (10x10x10m) is generated and the conductance is log-normally distributed with a mean value of 10^{-8} m^2 and a standard deviation of σ=1 (Fig. 16a). Within the cubic lattice network, a spherical constant-pressure outer boundary is created with hydraulic head difference of 2m between the injection point and the boundary, and the resulting distribution of pressure head is shown in Fig. 16b and the steady state flow solution is computed and the resulting flow rate distribution is shown in Fig. 16c. For better visualization, dominant channels with higher flow rate are plotted in Fig. 16d by making the low flow rate channels transparent (i.e., not shown). The so-called sparse channel networks can be created by eliminating very low flow channels to decrease the complexity and computational demands of the fracture system for further study. Pychan3D (Dessirier et al., 2018) can easily be modified to create these sparse networks based on cut-off threshold values of flow or any other parameters. Methods such as this may prove very useful when the network consists of thousands of fractures, representing a realistic site.

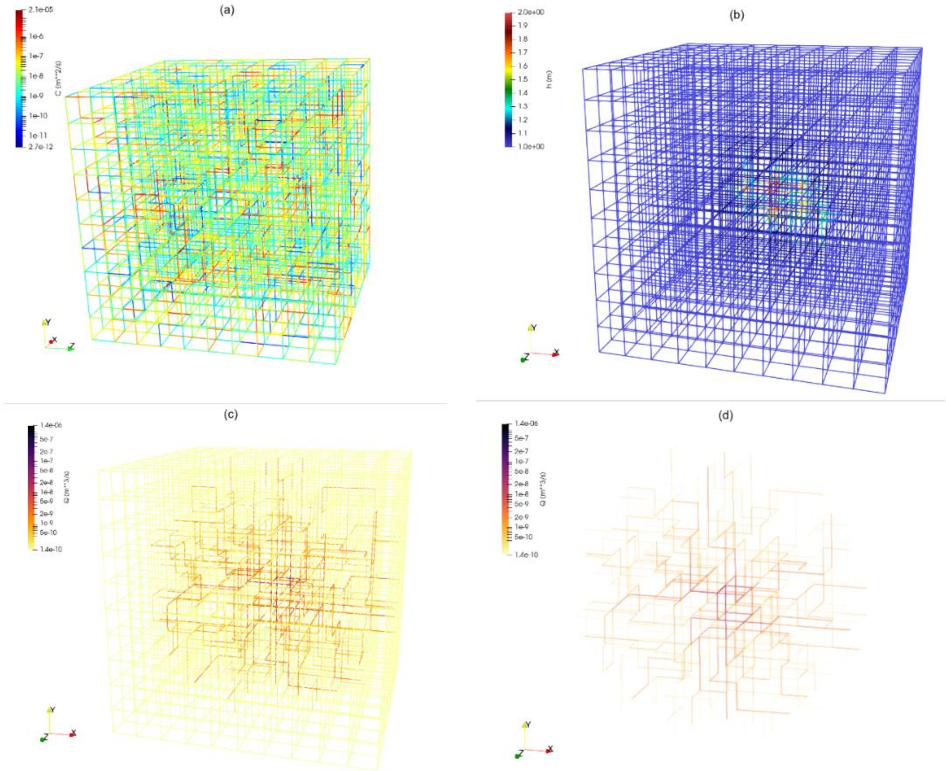

Fig. 16 Three-Dimensional channel network Geometry (a) conductance distribution, (b) hydraulic head distribution, (c) flow rate distribution, (d) channel network showing only channels of dominant flow

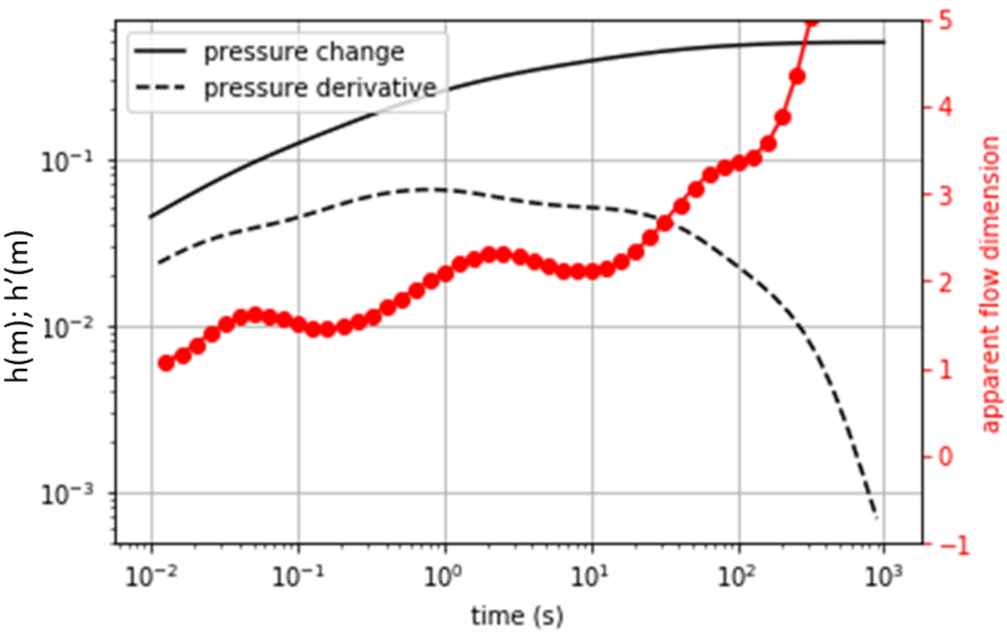

Fig. 17 Pressure and AFD variation against time in constant flow transient test in 3D network

Transient flow response of this 3D lattice network is investigated by performing a constant flow rate test at the centre node. With a constant pressure applied at the outer boundaries, the pressure and AFD variation are plotted with respect to injection time in Fig. 17. It is evident in this figure that AFD starts with n=1, try to stabilize at n=1.5 (bilinear flow) and then goes to n=2 (radial) and 3 (spherical) before hitting the boundary. This study is performed primarily to demonstrate the use of the model to simulate the multidimensional channel network to solve steady state and transient problems.

3.5 Application of transient AFD model to a site-specific fracture network data

After the previous studies in idealized systems, it is of interest to study realistic site data as well. Extensive data sets exist from Forsmark site in Sweden (Selroos et al. 2002). This is site investigated by the Swedish Nuclear Fuel and Waste Management Company (SKB) for the purpose of final disposal of high-level nuclear waste. The site is of low-conductivity crystalline rock and has been extensively characterized in multiple investigation phases (SKB, 2008). To demonstrate the practical application of the AFD model, the approach is used to examine the transient pressure response in a fracture network generated with a data from this site, Sweden. Geometric and hydraulic attributes of the fractures are derived from repository scale DFN models reported by SKB (SKB, 2011), and a corresponding channel network model is built by Sharma et al. (2022) using the approach described by Cacas et al. (1990). The generated 3D fracture network has 3276 fractures and 4353 fracture intersections in a 0.1 km^3 domain, based on which a channel network model (CNM) is developed using the Pychan3D code. Since isolated and dead-end fractures and fracture clusters do not participate in the flow, they are identified and removed from the original network and a hydraulically active backbone structure is obtained (Sharma et al., 2022) as shown in Fig. 18.

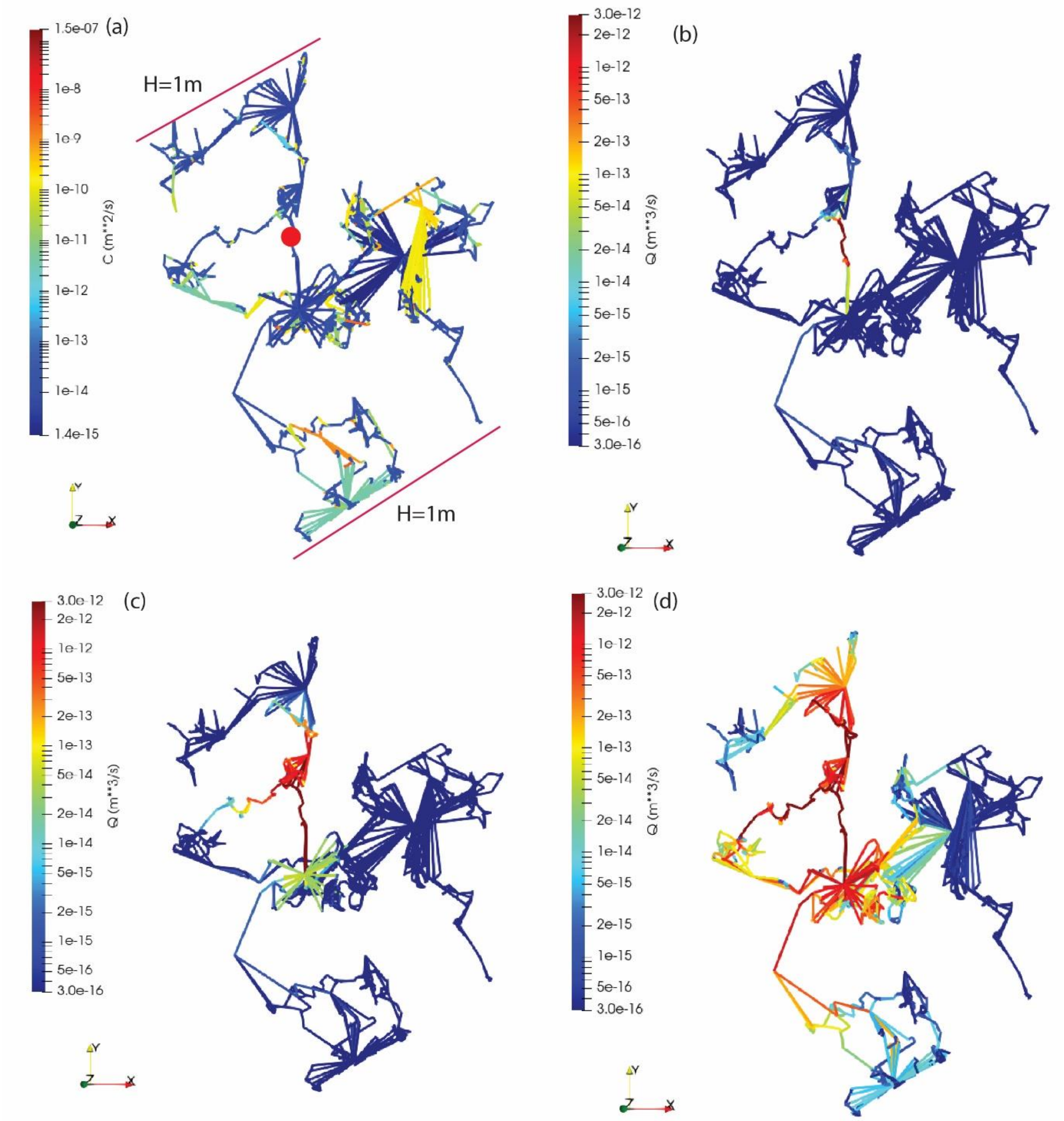

Fig. 18 A site-specific channel network model. (a) Conductance Distribution, (b) Pseudo steady state flow rate at injection time, $t_d=2x10^2$, (c) at $t_d=1.3\ x10^4$, and (d) at $t_d=2x10^5$.

To simulate a transient well test, in Fig. 18a, the outer NW and SE boundaries, representing nearby fault zones, were set at constant hydraulic head of 1m and water was injected at the constant rate of $1x\ 10^{-6}\ m^3/s$ at a location shown by red dot near the centre of the domain. In this study, the injection time (t_D) is scaled as t/S where S is the storativity of the flow medium. The pseudo-steady state flow rate distribution at different dimensionless times is shown in the Fig. 18b, c, and d. To evaluate the effect of the boundary conditions in an AFD plot, an additional calculation was made by setting the NW and SE boundaries as closed boundaries, which will result in AFD=0 at the large time limit. The obtained apparent flow dimension is shown in Fig. 19. The figure shows that the flow starts with dimension one and gradually changes depending on the flow geometry and conductance of the channels encountered by the pressure front before it hits the boundary. The presence of the specified pressure head boundary as open or closed is observed when flow dimension either rises very sharply at large time to a value of 5 or more (Fig. 19a), or goes to 0 (Fig. 19b). The flow dimension study using channel network shown in Fig. 18 unveils two AFD peaks between the early time AFD of 1 and the late time when the boundary effect sets in. The first AFD peak has a value of 2.1 at about $t_D=10^4$, and the second AFD peak occurs at about $t_D=10^6$. To account for the impact of the boundary condition, the value of the second peak is estimated to be 2.8 by taking the average of 3.3 and 2.4 from Fig. 19a and b respectively. In Fig. 18c and d, the flow passes through the clusters precisely at the same time (t_D) when AFD peaks observed in Fig. 19. The result can well be explained by the presence of the two clusters of channels on the two sides of the injection point (see Fig.18 a).

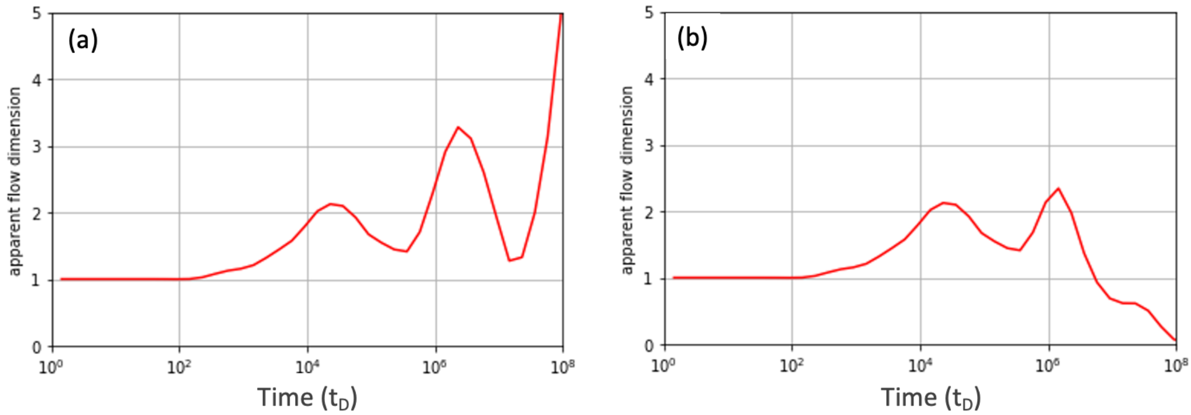

Fig. 19 AFD as a function of time, t_D (t/S) (a) with open boundary, and (b) close boundary for a site-specific study

The AFD behaviour as shown in Fig. 19 may give very useful insight into the changes in conductivity in space due to branching channels or channels with a larger conductance. The observation that the first peak is smaller than the second suggests that, along the route of the pressure pulse, it hits the smaller cluster first and then the larger cluster. If we compare these results with the correlation of conductance increase versus AFD developed in Fig. 4, the first and second peaks may indicate, respectively, encountering first a channel cluster with one order of magnitude larger conductance and then a second cluster with one-and-half orders of magnitude larger conductance. Further work may involve multiple injection tests at different locations and aggregate the results. In this way, the AFD method has the potential of providing extra information useful in characterizing the heterogeneity of the flow system.

On principle, S in the scaled time t_D=t/S shown in Fig. 19 can be estimated from pressure tests or interference tests using e.g., Theis type curve fitting method. It can also be calculated from a detailed analysis of fracture geometry of the network assuming a fracture storativity value, which however is strongly dependent on in-situ conditions at the site and can vary by several orders of magnitude (Rutqvist et al., 1998). Investigations on this issue are beyond the scope of the present demonstrative application and the time will be simply presented as t_D = t/S in Fig. 19. Different storativity values would move the position of the curve horizontally, but would show the same changes of AFD, which is the focus of our study.

4. Discussion and Conclusion

Flow dimensional analysis in fractured subsurface rock can be quite useful in understanding the system's heterogeneity structure. Since the majority of the flow regimes are non-radial (Ferroud et al. 2018), oversimplified analytical flow models may not be appropriate for studying fractured rock systems. This article discusses the transient testing technique for determining flow dimension in various scenarios, including the real-site case. A flow dimension analysis for a heterogeneous fracture network system was conducted utilizing a channel network model built using the pychan3D model. The study systematically proceeds from idealized 1D, 2D and 3D systems to a field case based on real data.

Our results in the 1D cases demonstrate that the AFD substantially changes as a function of channel conductance variation. When encountering a channel with greater conductance the AFD first abruptly increases before decreasing again to AFD=1. Conversely, when the flow is encountering a channel with lower conductivity, a clear dip in the AFD is observed. A systematic relationship correlating the magnitude of the conductance contrast and the magnitude of the upsurge/dip in the apparent flow dimension was established from the results (Fig. 4). Such a relationship appears to be useful to estimate the permeability variability in the flow domain from the results of transient well tests even in more complex situations.

The study was next extended to 2D domains. Heterogeneity was introduced statistically through conductance distributions with different standard deviation (σ) values. From ensemble averages of 50 realizations, it can be seen that for all σ values the AFD starts from a value of 1, indicating an early-time channelized flow near the borehole. Then, for low σ values (0 and 1) the AFD then converges towards 2, indicating that the flow is taking place radially throughout the system. For higher σ values the AFD does not stabilize at the value of 2 but ranges between 1 and 2, indicating a more channelized flow. The AFD for individual realizations is highly oscillating, with more oscillations and oscillations with higher amplitude with increasing σ. In field situations, such single realizations (corresponding to a single well test) could be used to observe the variation of conductance as the pressure front proceeds through the rock medium, according to the relationship presented in Fig. 4. If, instead, a number of realizations (corresponding to a number of well tests at different locations in the same network) are available, an ensemble mean could give an indication of the overall heterogeneity characteristics of the system.

A study was also conducted for a geometrically specified (deterministic) heterogeneity introduced into the 2D stochastic network. This was implemented by considering a linear zone of constant width within which the conductances were made significantly greater than that of the surrounding area. As to be expected for σ=0, the flow is found to be channelled through the high conductive linear zone, while for the σ=1 case, two degrees of channelized flow was observed: a primary channelization occurs in the linear zone and a secondary channelization also occurs within this zone due to the local conductance variability.

As the next step, the study was extended to 3D channel networks. In this case the channels have conductance values that follow a lognormal distribution with σ=1. As could be expected, the AFD in this case first starts with n=1, then successively proceeding to n=1.5, 2 and 3, when the flow becomes more space-filling and is going from bilinear to radial and spherical before finally encountering the boundary.

After these idealized cases, the study was extended to investigate the AFD in a set of actual site-specific fracture data (Sharma et al., 2022) from Forsmark, Sweden (Fig. 18). Here two peaks were observed in the AFD variation before the onset of the boundary effects. The behaviour could be explained by the presence of two main clusters of channels in the flow domain on the two sides of the injection point. When compared with the correlation between conductance contrast and AFD presented in Fig. 4, the two channel clusters may represent a conductance increase of 1 and 1.5 orders of magnitude respectively. If such transient well test data were available from several injection wells at different locations in the channel network, a joint AFD analysis of all results may provide useful data in the characterization of flow heterogeneity of the domain.

It should be emphasized that characterizing the heterogeneity structure of a flow domain, especially for fractured rock, is a challenging task. It requires multiple and complementary inputs from different types of data, such as fracture mapping on outcrops or tunnel surfaces, downhole imaging of fractures on borehole walls, flow (dilution) tests, single hole pressure tests, multiple hole interference tests, and tracer tests. The AFD analysis of transient pressure data over a long-time frame is an additional input that will help in this effort.

The main limitation and challenge of the AFD approach is the use of pressure derivatives in its analysis, which are very sensitive to minor variations in pressure data. Perhaps this can be alleviated by the use of data smoothing techniques and/or joint analysis of transient pressure data from multiple injection points in the flow domain and multiple repeated well tests from the same well. Another limitation is the time scale required for the pressure transient tests, which strongly depends on the overall permeability and storativity of the flow domain. Thus, the time to observe AFD variations may be too short (too fast) or too long to make this method practical in some field applications.

Finally, it should be noted that determination of hydraulic properties of a flow domain by assuming uniform properties and ignoring its heterogeneity structure may lead to significant errors, unless the heterogeneity is of very small range compared with the size of flow domain of interest. For fractured rocks and even for many aquifer systems, this assumption may well be invalid. The present paper presents a systematic study with some insight gained on the particular AFD approach, and further work will be carried out to address its limitations and better define its ranges of applicability under field conditions.

Acronyms and symbols

GRF	Generalized Radial Flow
AFD	Apparent Flow Dimension
RMS	Root mean square
DFN	Discrete Fracture Network
CNM	Channel network model
C	Conductance
Q	Flow Rate
h	Pressure drawdown/build up
T	Transmissivity
w	Width of the channel
L	Length of the channel
Mc	Laplacian matrix
Bc	Vector of boundary condition
n	Flow dimension
h'	Pressure derivative
t	time
V^*	Slope of pressure derivative
t_d	Scaled injection time
S	Storativity
N	nodes
σ	Standard deviation

Acknowledgements

The authors would like to express their gratitude to Joel Geier of Clearwater Hardrock Consulting (USA) for sharing data, as well as to Osvaldo Pensado and Stuart Stothoff of Southwest Research Institute for discussions during the course of this study. The authors would like to acknowledge funding from Swedish Radiation Safety Authority (SSM) for supporting this research.

Conflicts of interest

The authors have no conflicts of interest.

References

Barker, J. A. (1988). A generalized radial flow model for hydraulic tests in fractured rock. *Water Resources Research*, *24*(10), 1796–1804. https://doi.org/10.1029/WR024i010p01796

Black, J. H., Woodman, N. D., & Barker, J. A. (2017). Ecoulement d'eau souterraine au sein d'ouvertures dans les roches cristallines fracturées: une interprétation basée sur de longs chenaux. *Hydrogeology Journal*, *25*(2), 445–463. https://doi.org/10.1007/s10040-016-1511-y

Bourdet, D., Whittle, T. M., Douglas, A. A., & Pirard, Y. M. (1983). New Set of Type Curves Simplifies Well Test Analysis. *World Oil*, *196*(6), 1–7.

Cacas, M. C., Ledoux, E., Marsily, G., Barbreau, A., Calmels, P., Gaillard, B., & Margrita, R. (1990). Modelling fracture flow with a stochastic discrete fracture network: Calibration and validation, 2: the transport model. *Water Resources Research*, *26*(3), 491–500.

Chow, V. Te. (1952). On the determination of μ. In *American Geophysical Union* (Vol. 33, pp. 397–404).

Cinco, H., Samaniego V., F., & Dominguez A., N. (1978). Transient Pressure Behavior for a Well With a Finite-Conductivity Vertical Fracture. *Society of Petroleum Engineers Journal*, *18*(04), 253–264. https://doi.org/10.2118/6014-PA

Delay, F., Porel, G., & Bernard, S. (2004). Analytical 2D model to invert hydraulic pumping tests in fractured rocks with fractal behavior. *Geophysical Research Letters*, *31*(16), 2–5. https://doi.org/10.1029/2004GL020500

Dessirier, B., Tsang, C. F. C. F., & Niemi, A. (2018). A new scripting library for modeling flow and transport in fractured rock with channel networks. *Computers and Geosciences*, *111*(April 2017), 181–189. https://doi.org/10.1016/j.cageo.2017.11.013

Doe, T. (1991). Fractional dimension analysis of constant-pressure well tests. *Society of Petroleum Engineers, SPE Pap*, *22702*, 461–467.

Doe, T., & Geier, J. (1990). *Interpretation of fracture system using well test data*.

Ferroud, A., Chesnaux, R., & Rafini, S. (2018). Insights on pumping well interpretation from flow dimension analysis: The learnings of a multi-context field database. *Journal of Hydrology*, *556*, 449–474. https://doi.org/10.1016/j.jhydrol.2017.10.008

Ferroud, A., Rafini, S., & Chesnaux, R. (2019). Using flow dimension sequences to interpret non-uniform aquifers with constant-rate pumping-tests: A review. *Journal of Hydrology X*, *2*, 100003. https://doi.org/10.1016/j.hydroa.2018.100003

Gringarten, A. C. (2008). From straight lines to deconvolution: The evolution of the state of the art in well test analysis. *SPE Reservoir Evaluation and Engineering*, *11*(1), 41–62. https://doi.org/10.2118/102079-pa

Gringarten, A. C., Ramey Jr., H. J., & Raghavan, R. (1974). Unsteady-State Pressure Distributions Created by a Well With a Single Infinite-Conductivity Vertical Fracture. *Society of Petroleum Engineers Journal*, *14*(04), 347–360. https://doi.org/10.2118/4051-PA

Gylling, B., Moreno, L., & Neretnieks, I. (1999). The channel network model - A tool for transport simulations in fractured media. *Ground Water*, *37*(3), 367–375. https://doi.org/10.1111/j.1745-6584.1999.tb01113.x

Kuusela-Lahtinen, A., & Poteri, A. (2010). Interpretation of flow dimensions from constant pressure injection test. *Working Report*, 2010–2035.

Kuusela-Lahtinen, A., Niemi, A., & Luukkonen, A. (2002). Flow dimension as an indicator of hydraulic behavior in site characterization of fractured rock. *Groundwater*, *41*(3), 333–341.

Li, S. C., Xu, Z. H., & Ma, G. W. (2014). A Graph-theoretic Pipe Network Method for water flow simulation in discrete fracture networks: GPNM. *Tunnelling and Underground Space Technology*, *42*, 247–263.

https://doi.org/10.1016/j.tust.2014.03.012

Mahmoudzadeh, B., Liu, L., Moreno, L., & Neretnieks, I. (2013). Solute transport in fractured rocks with stagnant water zone and rock matrix composed of different geological layers - Model development and simulations. *Water Resources Research*, *49*(3), 1709–1727. https://doi.org/10.1002/wrcr.20132

Miller, F. G. (1962). Theory of Unsteady-State Influx of Water in Linear Reservoirs. *J. Inst. Pet.*, *48*(467), 365–379.

Moreno, L., & Neretnieks, I. (1993). Fluid flow and solute transport in a network of channels. *Journal of Contaminant Hydrology*, *14*(3–4), 163–192. https://doi.org/10.1016/0169-7722(93)90023-L

Moreno, L., Crawford, J., & Neretnieks, I. (2006). Modelling of transport in fractures with complex matrix properties. In *Materials Research Society Symposium Proceedings* (Vol. 932, pp. 267–274). https://doi.org/10.1557/proc-932-98.1

Moye, D. G. (1967). Diamond drilling for foundation exploration. *Civ. Eng. Trans.*, 95–100.

National Research Council. (1996). *Rock fractures and fluid flow: contemporary understanding and applications*. National Academies Press.

Neretnieks, I. (2006). Channeling with diffusion into stagnant water and into a matrix in series. *Water Resources Research*, *42*(11). https://doi.org/10.1029/2005WR004448

Odling, N. E., West, L. J., Hartmann, S., & Kilpatrick, A. (2013). Fractional flow in fractured chalk; A flow and tracer test revisited. *Journal of Contaminant Hydrology*, *147*, 96–111. https://doi.org/10.1016/j.jconhyd.2013.02.003

Rafini, S., & Larocque, M. (2009). Insights from numerical modeling on the hydrodynamics of non-radial flow in faulted media. *Advances in Water Resources*, *32*(8), 1170–1179. https://doi.org/10.1016/j.advwatres.2009.03.009

Rafini, S., Chesnaux, R., & Ferroud, A. (2017). Une étude numérique des réponses d’essais de pompage d’aquifères contigus. *Hydrogeology Journal*, *25*(3), 877–894. https://doi.org/10.1007/s10040-017-1560-x

Renard, P., Glenz, D., & Mejias, M. (2009). Understanding diagnostic plots for well-test interpretation.

Hydrogeology Journal, *17*(3), 589–600. https://doi.org/10.1007/s10040-008-0392-0

Rutqvist, J., Noorishad, J., Tsang, C., & Stephansson, O. (1998). Determination of fracture storativity in hard rocks using high-pressure injection testing. *Water Resources Research*, *34*(10), 2551–2560.

Selroos, J. O., Walker, D. D., Anders, S., Gylling, B., & Follin, S. (2002). Comparison of alternative modelling approaches for groundwater flow in fractured rock. *Journal of Hydrology*, *257*, 174–188.

Shahkarami, P., Liu, L., Moreno, L., & Neretnieks, I. (2016). The effect of stagnant water zones on retarding radionuclide stransport in fractured rocks: An extension to the Channel Network Model. *Journal of Hydrology*, *540*, 1122–1135. https://doi.org/10.1016/j.jhydrol.2016.07.031

Sharma, K. M., Geier, J., Dessirier, B., Stothoff, S., Pensado, O., Tsang, C., & Niemi, A. (2022). An investigation into flow and transport in a complex fracture network in deep crystalline rock based on a channel network model. Gdansk, Poland: The XXIV International Conference on Computational Methods in Water Resources (CMWR).

SKB. (2008). *Site description of Forsmark at completion of the site investigation phase - SDM-Site Forsmark, Technical Report TR-08-05*. Retrieved from https://skb.se/publication/1868223/TR-08-05.pdf

SKB. (2011). *SR-Site main report. SKB Technical Report TR-11-01*. Stockholm.

Theis, C. V. (1935). The relation between the lowering of the Piezometric surface and the rate and duration of discharge of a well using ground-water storage. *Eos, Transactions American Geophysical Union*, *16*(2), 519–524. https://doi.org/https://doi.org/10.1029/TR016i002p00519

Verbovšek, T. (2009). Influences of Aquifer Properties on Flow Dimensions in Dolomites. *Groundwater*, *47*(5), 660–668. https://doi.org/https://doi.org/10.1111/j.1745-6584.2009.00577.x

Walker, D., & Roberts, R. (2003). Flow dimensions corresponding to hydrogeological conditions. *Water Resources Research*, *39*(12), 1349.

Walker, D. D., Cello, P. A., Valocchi, A. J., & Loftis, B. (2006). Flow dimensions corresponding to stochastic models of heterogeneous transmissivity. *Geophysical Research Letters*, *33*(7). https://doi.org/https://doi.org/10.1029/2006GL025695

1